Deformable Object Modelling Through Cellular Neural Network

Yongmin Zhong[1], Bijan Shirinzadeh[1], Gursel Alici[2], Julian Smith[3] and Danny Oetomo[1]

[1]*Robotics & Mechatronics Research Laboratory*
Monash University
VIC 3800, Australia

[2]*School of Mechanical, Materials, and Mechatronics Engineering*
University of Wollongong
2522 NSW, Australia

[3]*Department of Surgery*
Monash Medical Centre
Monash University
VIC 3800, Australia

Yongmin.Zhong@eng.monash.edu.au
Bijan.Shirinzadeh@eng.monash.edu.au

gursel@uow.edu.au

Julian.Smith@med.monash.edu.au

Abstract

This paper presents a new methodology for the deformable object modelling by drawing an analogy between cellular neural network (CNN) and elastic deformation. The potential energy stored in an elastic body as a result of a deformation caused by an external force is propagated among mass points by the non-linear CNN activity. An improved autonomous CNN model is developed for propagating the energy generated by the external force on the object surface in the natural manner of heat conduction. A heat flux based method is presented to derive the internal forces from the potential energy distribution established by the CNN. The proposed methodology models non-linear materials with non-linear CNN rather than geometric non-linearity in the most existing deformation methods. It can not only deal with large-range deformations due to the local connectivity of cells and the CNN dynamics, but it can also accommodate both isotropic and anisotropic materials by simply modifying conductivity constants. Examples are presented to demonstrate the efficacy of the proposed methodology.

1. Introduction

Virtual reality based surgery simulation is expected to provide benefits in many aspects of surgical procedure training and evaluation. To this end, a significant amount of research efforts have been dedicated to simulating the behaviours of deformable objects. These research efforts can be divided into two classes. One is focused on real-time simulation such as mass-spring models [1, 2] and spline surfaces used for deformation simulation and visualization [3, 4]. The advantage of this method is that the computation is less time consuming and the algorithm is easier to be implemented. However, the method does not allow accurate modelling of material properties, and more importantly, increasing the number of springs leads to a stiffer system. The other method focuses on deformation modelling using techniques such as Finite Element Method (FEM) [5, 6] and Boundary Element Method (BEM) [7, 8]. In FEM or BEM, rigorous mathematical analysis based on continuum mechanics is applied to accurately model the mechanical behaviours of deformable objects. However, these methods are computationally expensive and are typically simulated off-line. The pre-calculation [7], matrix condensation [9], the space and time adaptive level-of-detail [10] and explicit finite element [11] techniques are used to enhance the computational performance.

In general, most of the existing methods for deformable object modelling are fully built on a linear elastic model to describe the deformation, while the behaviours of deformable objects such as human tissues and organs are extremely nonlinear [12, 13]. The common deformation methods, such as mass-spring, FEM and BEM, are mainly based on linear elastic models because of the simplicity of linear elastic models, and also because linear elastic models allow reduced runtime computations. However, linear elastic models cannot accommodate the large-range geometric deformations and the displacements are only allowed to be less than 10% of the deformable object size [12, 14]. Although few methods based on the nonlinear elastic model can handle the large-range deformations [15], the use of quadric strains generally requires a very expensive computation for real-time simulation. The runtime assembly of all the force terms for every element limits the interactivity to only a few hundred elements. In addition, only geometric nonlinearity is modelled rather than non-linear material properties, extra work often needs to be performed for anisotropic deformations.

This paper presents a new methodology for the deformable object modelling by drawing an analogy between cellular neural network (CNN) and elastic deformation. The deformation is formulated as a dynamic CNN. The potential energy stored due to a deformation caused by an external force is calculated and treated as the energy injected into the system, as described by the law of conservation of energy. An improved autonomous CNN model is developed for propagating the energy generated by the external force among mass points through the local connectivity of cells and the CNN dynamics. The improved CNN model provides a natural manner for energy propagation since the local connectivity of cells acts as the local interaction of heat equation. A heat flux based method is presented to derive the internal forces from the potential energy distribution established by the CNN. The methodology can not only deal with large-range deformations due to the local connectivity of cells and the CNN dynamics, but it can also accommodate both isotropic and anisotropic materials easily through simply modifying the conductivity constants.

There are several investigations that combine neural network with deformable modelling [16, 17]. However, in these methods, neural networks are mainly used to determine the parameters of mass-spring models. To the best of our knowledge, this study is the first to

directly use neural network techniques to mimic the behaviours of deformable objects under externally applied loads. The contribution of this paper is that non-linear materials are modelled with non-linear CNN rather than geometric non-linearity, and CNN techniques are used to naturally propagate the energy generated by the external force and further to extrapolate the internal forces from the natural energy distribution for deformations.

2. Design of CNN Model

2.1 CNN Analogy CNN is a dynamic nonlinear circuit composed by locally coupled, spatially recurrent circuit units called cells, which contain linear capacitors, linear resistors, and linear/nonlinear current sources. One significant feature of CNN, as well as the basic difference from other neural networks, is the local connectivity of cells [18], i.e. any cell in CNN is connected only to its neighbouring cells. Adjacent cells directly interact with each other. Cells not directly connected to each other have indirect effect because of the propagation effects of the continuous-time dynamics of CNN. The activity of a cell is propagated to other cells through the local connectivity of cells and the time-continuous dynamics. Therefore, CNN provides a manner for modelling the physical process of energy propagation.

Another significant feature of CNN is that the individual cells are non-linear dynamical systems, but that the coupling between them, i.e. the local connectivity of cells, is linear [19]. The feature makes CNN very suitable for modelling non-linear materials since CNN conserves the physical properties of the continuous structure.

In addition, given the initial state and the external environment, CNN activity is only determined by the local connectivity of cells. The local connectivity of cells is similar to the internal force since the deformation is only determined by the internal force under the given external force and the initial state.

Further, CNN offers an incomparable computation speed due to the collective and simultaneous activity of all cells. The computation advantage of CNN is very suitable for real-time the computation requirement of deformable object simulation.

Deformation of deformable objects is actually a process of propagating the energy generated by the external force. The process of energy propagation can be described by a CNN, in which the activity of a cell is propagated to others through the local connectivity of cells and the CNN dynamics. In the proposed CNN analogy, the deformation of deformable objects is treated as the activity of a CNN. The object surface with locally connected mass points is treated as a CNN with locally connected cells. The energy generated by the external force is treated as the current source of the contact cell. As a result of the CNN activity, the energy is propagated among mass points through the local connectivity of cells and a potential field is further developed on the object surface. The activity of a cell always follows the potential change, moving from a high potential energy point to a low potential energy point. Therefore, such a CNN with the current source, the local interaction generated from the local connectivity of cells and the activity can be seen as a communication medium among an external force, internal forces and deformation.

2.2 CNN Architecture A CNN model can be applied to different grid types. Without loss of generality, we consider a CNN on a rectangular grid with M rows and N columns. Each node on the grid is occupied by a cell. The dynamics of the array of M×N cells is described by the following equation and conditions [18]:

$$C\frac{dv_{xij}(t)}{dt} = -\frac{1}{R_x}v_{xij}(t) + \sum_{(k,l)\in N_r(i,j)} A(i,j;k,l)v_{ykl}(t) + \sum_{(k,l)\in N_r(i,j)} B(i,j;k,l)v_{ukl} + I_{ij} \quad (1a)$$

$$v_{yij}(t) = \frac{1}{2}(|v_{xij}(t)+K| - |v_{xij}(t)-K|), \quad K \geq 1 \quad (1b)$$

$$|v_{xij}(0)| \leq 1, \quad |v_{uij}| \leq 1 \quad (1c)$$

$$N_r(i,j) = \{(a,b) \mid \max\{|a-i|, |b-j|\} \leq r, \; 1 \leq a \leq M, \; 1 \leq b \leq N\} \quad (1d)$$

$$(1 \leq i \leq M; \; 1 \leq j \leq N)$$

where *(i, j)* refers to the cell associated with the node under consideration, *(k,l)* to a cell in the neighborhood of the cell *(i, j)*, namely $N_r(i, j)$, within a radius *r* of the cell *(i, j)* (r=1 for simplicity). *C* is the capacitance of a linear capacitor, R_x is the resistance of a linear resistor, and *I* is the current of the independent linear/nonlinear current source. *A* is the feedback template and *B* is the control template. The $v_{uij}(t)$, $v_{xij}(t)$, and $v_{yij}(t)$ denote the input, state and output of the cell *(i,j)* at the time *t*, respectively. $v_{yij}(t)$ is a non-linear sigmoid function of $v_{xij}(t)$, and it is bounded by a constant K, which is equal to or greater than one.

Without inputs, Eq. (1) becomes an autonomous CNN;

$$C\frac{dv_{xij}(t)}{dt} = -\frac{1}{R_x}v_{xij}(t) + \sum_{(k,l)\in N_r(i,j)} A(i,j;k,l)v_{ykl}(t) + I_{ij} \quad (2)$$

3. Construction of CNN Model

3.1 Current Source Formulation When a deformable object is deformed under an external force, there is a displacement observed. The deformation is the consequence of the work done by the external force. According to the law of conservation of energy, the work done by the external force can be transformed into an equivalent electric energy at the contact point. Therefore, the current source I is

$$I = \frac{\vec{F} \bullet \vec{S}}{A_F} \quad (3)$$

where $\vec{F}$ is the external force, $\vec{S}$ is the displacement and A_F is the area on which the external force is applied.

If the external force is applied to a point or the area that the force is applied on is small, the current *I* may be regarded as the elastic strain energy density at the contact point:

$$I = \frac{1}{2}\sigma\varepsilon = \frac{1}{2}\sum_{i=1}^{3}\sum_{j=1}^{3}\sigma_{ij}\varepsilon_{ij} \quad (4)$$

where σ is the stress tensor and ε is the strain tensor at the contact point. The commonly used and simple strain tensor is linear Cauchy strain tensor described by:

$$\varepsilon = \frac{1}{2}\left(\frac{\partial u_i}{\partial x_j} + \frac{\partial u_j}{\partial x_i}\right) \quad (5)$$

A straight forward approach that leads to a linear relationship between these two tensors is provided by the Hooke's law:

$$\sigma = \mathbf{C}\varepsilon \quad (6)$$

where **C** is a tensor approximating the constitutive law of a material. For isotropic materials, **C** has only two independent coefficients, i.e. Young's Modulus and Poisson's Ratio.

From Eq. (6), we can deduce the displacement from the given external force and subsequently the current *I* can be obtained.

In most of CNN applications, the current source of each cell has the same value. For our purpose, the energy generated by the external force is treated as a current source and propagated to other mass points along the object surface. Therefore, the obtained current source is set only at the contact cell of the external force, and the current source values of other cells are set to zero.

3.2 Heat equation Heat conduction is a natural description of energy propagation according to the inherent properties of materials, i.e. the thermal conductivity. The well known heat equation is

$$k_u \frac{\partial^2 \varphi(u,w,t)}{\partial u^2} + k_w \frac{\partial^2 \varphi(u,w,t)}{\partial w^2} = \frac{\partial \varphi(u,w,t)}{\partial t} \quad (7)$$

where $\varphi(u,w,t)$ is the potential of the observed point with coordinates u and w at time t, k_u and k_w are the conductivity of the observed point in the *u* and *w* directions, respectively.

For isotropic materials, there is $k_u = k_w = k$. Therefore, Eq. (7) becomes:

$$k\nabla^2 \varphi(u,w,t) = \frac{\partial \varphi(u,w,t)}{\partial t} \quad (8)$$

where ∇^2 is the Laplace operator.

The inherent analogies between the CNN dynamic equation and the heat equation have been made evident in the CNN literature [18, 20]. Both the CNN and the heat equation describe the time-continuous dynamics and have the same property that their dynamic behaviours depend only on their spatial local interactions [18]. Therefore, the local connectivity of cells is formulated as the local interaction of the heat equation to make the CNN has the similar natural behaviour of energy propagation as heat conduction. To clarify the local interaction of the heat equation and further to draw the analogy between the heat equation and the CNN, the heat equation has to be discretized on the 3D object surface.

3.3 Discretization of heat equation on a rectangular grid The discretization of the heat equation on a rectangular grid is straightforward. The heat equation at each internal node can be established by discretizing the Laplace operator in Eq. (8) using a finite-difference scheme. For the point $\vec{P}_{ij}$ shown in Fig. 2, the discrete heat equation is shown in Eq. (9).

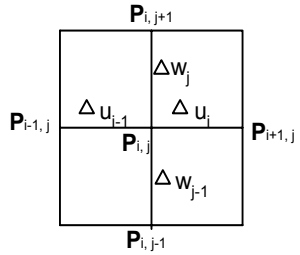

Fig. 1 Heat equation discretization on a rectangular net

$$\frac{2k\varphi_{i+1,j}(t)}{\Delta u_i(\Delta u_{i-1}+\Delta u_i)} + \frac{2k\varphi_{i-1,j}(t)}{\Delta u_{i-1}(\Delta u_{i-1}+\Delta u_i)} + \frac{2k\varphi_{i,j+1}(t)}{\Delta w_j(\Delta w_{j-1}+\Delta w_j)} + \frac{2k\varphi_{i,j-1}(t)}{\Delta w_{j-1}(\Delta w_{j-1}+\Delta w_j)} - \frac{2k\varphi_{i,j}(t)}{\Delta u_{i-1}\Delta u_i} - \frac{2k\varphi_{i,j}(t)}{\Delta w_{j-1}\Delta w_j} = \frac{\partial \varphi_{i,j}(t)}{\partial t} \quad (9)$$

$$\Delta u_{i-1} = \left\|\overrightarrow{P_{i-1,j}P_{i,j}}\right\| \qquad \Delta u_i = \left\|\overrightarrow{P_{i,j}P_{i+1,j}}\right\|$$

$$\Delta w_{j-1} = \left\|\overrightarrow{P_{i,j-1}P_{i,j}}\right\| \qquad \Delta w_j = \left\|\overrightarrow{P_{i,j}P_{i,j+1}}\right\|$$

where $\varphi_{i,j}(t)$ is the potential at point $\vec{P}_{i,j}$ at the time t, $\left\|\overrightarrow{P_{i-1,j}P_{i,j}}\right\|$ and other similar terms represent the magnitudes of the vector $\overrightarrow{P_{i-1,j}P_{i,j}}$ and other similar vectors.

With respect to Eq. (9), the discrete heat equation on a rectangular grid for anisotropic materials can be easily obtained.

3.4 Discretization of heat equation on a triangular grid

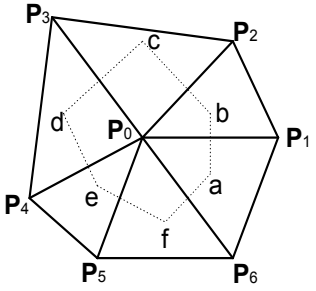

Fig. 2 Voronoi scheme for the heat equation discretization on a triangular net

For the heat equation discretization on a triangular net, a finite volume method [21] is used to aid discretizing the heat equation at each node. One straightforward finite volume method is Voronoi diagram [22], which derives the discretized equation at each node from the energy conservation law. Fig. 2 shows the finite volume constructed by the Voronoi scheme. The finite volume of point $\vec{P}_0$ is constructed by connecting each intersection points between the perpendicular

centerlines of each edges adjacent to point $\vec{P}_0$. The discretization equation at point $\vec{P}_0$ is shown in Eq. (10).

$$\begin{aligned}&\frac{kL_{ab}}{SL_{01}}[(\varphi_1(t)-\varphi_0(t)]+\frac{kL_{bc}}{SL_{02}}[\varphi_2(t)-\varphi_0(t)]+\\&\frac{kL_{cd}}{SL_{03}}[\varphi_3(t)-\varphi_0(t)]+\frac{kL_{de}}{SL_{04}}[\varphi_4(t)-\varphi_0(t)]+\\&\frac{kL_{ef}}{SL_{05}}(\varphi_5(t)-\varphi_0(t)]+\frac{kL_{fa}}{SL_{06}}(\varphi_6(t)-\varphi_0(t)]=\frac{\partial\varphi_0(t)}{\partial t}\end{aligned} \quad (10)$$

where $L_{mn}=\left\|\overrightarrow{P_mP_n}\right\|$ is the distance between two points $\vec{P}_m$ and $\vec{P}_n$, and S is the measure of the finite volume.

With respect to Eq. (10), the discrete heat equation on a triangular grid for anisotropic materials can be easily obtained.

3.5 Formulation for local connectivity of cells The right side of the discretized heat equation shows the local interaction of the heat equation clearly. The CNN templates that define the local connectivity of cells are obtained from the local interaction of the heat equation. For example, the analogy between the CNN Eq. (2) and the discretized heat equation Eq. (9) is evident by associating the state of a CNN cell $v_{xij}(t)$ with the heat potential $\varphi_{i,j}(t)$, and the CNN templates can also be obtained;

$$A=\begin{pmatrix}0 & \dfrac{2k}{\Delta w_j(\Delta w_{j-1}+\Delta w_j)} & 0\\ \dfrac{2k}{\Delta u_{i-1}(\Delta u_{i-1}+\Delta u_i)} & \dfrac{1}{R_x}-\dfrac{2k}{\Delta u_{i-1}\Delta u_i}-\dfrac{2k}{\Delta w_{j-1}\Delta w_j} & \dfrac{2k}{\Delta u_i(\Delta u_{i-1}+\Delta u_i)}\\ 0 & \dfrac{2k}{\Delta w_{j-1}(\Delta w_{j-1}+\Delta w_j)} & 0\end{pmatrix} \quad (11)$$

With reference to Eq. (11), the corresponding CNN templates can also be obtained from the other discretized heat equations for isotropic and anisotropic materials.

The solution of the heat equation needs initial values and boundary conditions. Therefore, the initial values and boundary conditions are also incorporated in the CNN model. The initial values of the heat equation can be directly associated with the initial state of the CNN. The simplest boundary condition is the Dirichlet boundary condition, i.e. the given boundary values. The Dirichlet boundary condition is realized by using some fixed-state cells.

Since the CNN model has no inputs (i.e. B=0), the constraint conditions Eq. (1c) can be easily satisfied by setting the initial value is zero.

4. Internal Force Derivation and Model Dynamics

4.1 Internal force derivation Potential functions provide an elegant method of describing internal forces based on point positions. For a potential function ϕ, the force exerted on a point $\vec{P}_i$ is due to the gradient of the potential energy ϕ with respect to the change in position, as described below.

$$\vec{f}=-\nabla_{\vec{P}_i}\phi \quad (12)$$

The potential field developed by the activity of the CNN describes the energy distribution on the object surface. The associated potential function is the output, which can be further written as v(u,w,t) since a cell corresponds to a mass point. Since the CNN has the similar behaviour with the heat equation, the internal force described as the negative gradient of the potential with respect to the change in position is actually heat flux;

$$f=-k\nabla_{\vec{P}_i}v \quad (13)$$

For anisotropic materials, Eq. (13) becomes

$$f=-\nabla_{\vec{P}_i}kv \quad (14)$$

The property of the local connectivity of cells is inherited by the internal force. An internal force exists between any two connected points and the internal force at a point is derived from the connected neighbouring points of this point. The force between any two connected points is calculated as follows:

Consider two adjacent points $\vec{P}_i$ and $\vec{P}_j$, where the potentials are $v_{\vec{P}_i}$ and $v_{\vec{P}_j}$, respectively. The potential at any point $\vec{P}$ on the edge between these two points is regarded as a function of the distance between the point $\vec{P}_i$ and the point $\vec{P}$. Therefore, the following relationships can be written:

$$v=v(l)\qquad l=\left\|\vec{P}-\vec{P}_i\right\| \quad (15)$$

Thus:

$$\nabla_{\vec{P}_i}v=\frac{dv}{dl}\nabla_{\vec{P}_i}l=-\frac{\left|v_{\vec{P}_j}-v_{\vec{P}_i}\right|}{\left\|\vec{P}_j-\vec{P}_i\right\|}\overrightarrow{P_iP_j} \quad (16)$$

where $\overrightarrow{P_iP_j}=\dfrac{\vec{P}_j-\vec{P}_i}{\left\|\vec{P}_j-\vec{P}_i\right\|}$ and $\left|v_{\vec{P}_j}-v_{\vec{P}_i}\right|$ is the magnitude of the potential change between the point $\vec{P}_i$ and the point $\vec{P}_j$.

Therefore, the force between the point $\vec{P}_i$ and the point $\vec{P}_j$ is

$$\vec{f}_{ij}=k\frac{\left|v_{\vec{P}_j}-v_{\vec{P}_i}\right|}{\left\|\vec{P}_j-\vec{P}_i\right\|}\overrightarrow{P_iP_j} \quad (17)$$

The internal force $\vec{g}_i$ at a given point $\vec{P}_i$ is the sum of the internal forces from all connected neighbor points of point $\vec{P}_i$.

$$\vec{g}_i=\sum_{j\in N(\vec{P}_i)}\vec{f}_{ij} \quad (18)$$

where $N(\vec{P}_i)$ is the connected neighbor points of $\vec{P}_i$, $\vec{f}_{ij}$ is the force between point $\vec{P}_i$ and its neighbor point $\vec{P}_j$.

4.2 Model dynamics When an external force is applied

to a deformable object, the contact point of the external force is replaced with a new position. As a result, the other points not influenced by the external force are in an unstable state. The energy generated by the external force is propagated among mass points through the local connectivity of cells to establish a new equilibrium state by generating the corresponding internal forces. Based on the equilibrium state, the new position of each point is obtained. The dynamic behaviour is governed by the Lagrangian equation of motion of each node:

$$m_i \frac{d^2 \vec{P}_i}{dt^2} + \gamma_i \frac{d\vec{P}_i}{dt} + \vec{g}_i = \vec{F}_i \qquad (19)$$

where $\vec{P}_i$ is the position vector of the node i, m_i and γ_i are the mass and damping constant of the node i, respectively. $\vec{g}_i$ is the net internal force applied to the node i at time t, and $\vec{F}_i$ is the external force applied to the node i at time t.

The solution of Eq. (19) can be computed either by an implicit integration scheme or an explicit integration scheme. Although the implicit integration has the advantage of being unconditionally stable, which means it allows large time steps to be used, it is computationally intensive and requires inverting a sparse matrix at each iteration [23]. Therefore, the explicit integration scheme [11, 15] is used to solve the Eq. (19). The advantage of the explicit scheme is that no matrix inversion is required for updating each vertex position.

5. Implementation Results and Discussions

A prototype system has been implemented for interactive deformable object simulation. A PHANToM haptic device is configured with the system to carry out the deformations of deformable objects with force feedback. Graphical and haptic rendering sre achieved by the OpenGL graphics library and the OpenHaptic Toolkit from Sensable Technologies, respectively. Experiments are conducted to investigate isotropic deformation, anisotropic deformation and the non-linear load-deformation of the model.

Fig. 3 illustrates the deformations of two isotropic material modelled with 400 mass points (conductivity = 0.4 and the damping = 10). Fig. 3(a) and (b) shows the deformation of an elliptic sphere. Fig. 3(c) and (d) shows the deformation of a cylindrical object.

The behaviours of anisotropic materials can be easily simulated by the proposed model through simply setting different conductivity values. Fig. 4 illustrates the deformations of anisotropic materials, where the red parts have a different conductivity value from the green part. As shown in Fig. 4(a) and (b), some of the red parts are also deformed correspondingly during the deformation process. Fig. 4(c) and (d) show that the red parts with a very low conductivity are not deformed by the external force.

The proposed method has been tested to determine if it exhibits non-linear load-deformation relationship. Eight materials that are modelled with different damping constants (from right to left in Fig. 5, the damping is 1.0, 2.0, 4.0, 5.0, 6.0, 7.0, 9.0 and 10.0, respectively) are tested. The deformation is calculated when the force applied to the model is increased at a constant rate. The results in Fig. 5 demonstrate that deformation varies non-linearly with the applied force.

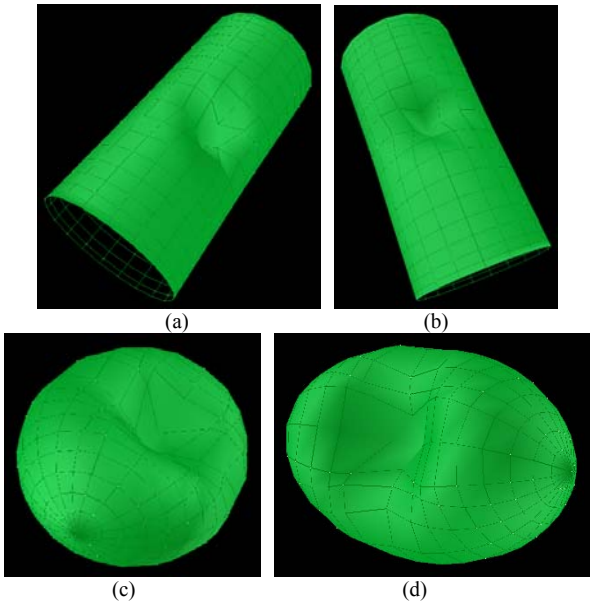

Fig. 3 Deformations of isotropic materials

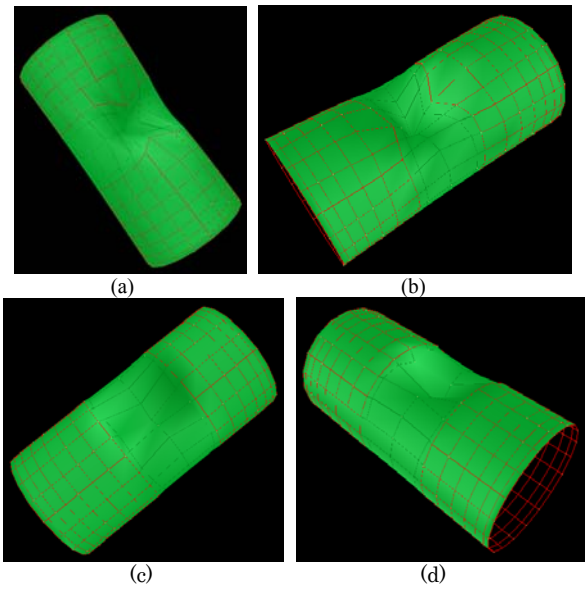

Fig. 4 Deformations of anisotropic materials

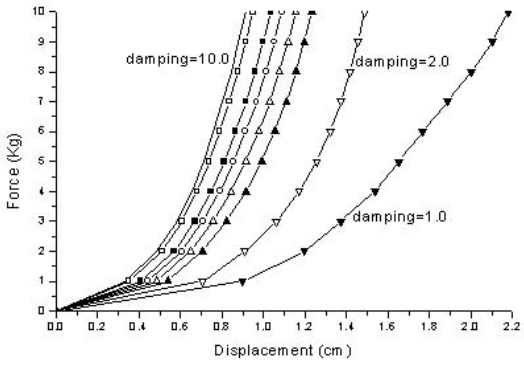

Fig. 5 Non-linear load-deformation relationship

Compared with most of the existing deformation

methods such as mass-spring, BEM and linear FEM, the methodology can perform large-range displacements through its non-linear load-deformation relationship. Compared with non-linear FEM such as [15], the CNN model is more easier to be formulated than the complex non-linear elastic model, and only surface mass points are involved in computation and rendering without any inside points while the interior has to be meshed and calculated in FEM. In addition, the methodology can easily accommodate anisotropic materials by simply setting conductivity constants while extra work has to be performed in both mass-spring and FEM.

6. Conclusions

This paper presents a new methodology to mimic the behaviours of deformable objects by establishing an analogy between CNN and elastic deformation. The contribution of this paper is that non-linear materials are modeled with non-linear CNN rather than geometric non-linearity, and CNN techniques are established to propagate the energy generated by the external force for extrapolating internal forces. An improved autonomous CNN model is developed for propagating the energy generated by the external force on the object surface in the natural manner of heat conduction. A method is presented for deriving the internal forces from the potential energy distribution. This proposed methodology can not only deal with large-range deformations due to the local connectivity of cells and the CNN dynamics, but also can accommodate both isotropic and anisotropic materials through simply modifying the conductivity constants.

Acknowledgments

This research is supported by Australian Research Council (ARC).

References

[1] C. Paloc, F. Bello, R. I. Kitney and A. Darzi, "Online multiresolution volumetric mass spring model for real time soft tissue deformation", Lecture Notes in Computer Science, vol. 2489, 2002, pp. 219-226

[2] K. Choi, H. Sun and P. A. Heng, "Interactive deformation of soft tissues with haptic feedback for medical learning", IEEE Transaction on Information Technology in Biomedicine, vol. 7, no. 4, 2003, pp.358-363

[3] U. Bockholt, W. Müller and G. Voss (etc.), Real-time simulation of tissue deformation for the nasal endoscopy simulator (NES), Computer aided surgery, vol. 4, no. 5, 1999, pp. 281-285

[4] J. S. Rotnes, J. Kaasa and G. Westgaard (etc.), "Realism in surgical simulators with free-form geometric modeling", International Congress Series, vol. 1230, 2001, pp. 1032-1037

[5] S. Cotin, H. Delingette and N. Ayache, "A hybrid elastic model allowing real-time cutting, deformations and force-feedback for surgery training and simulation", The Visual Computer, vol. 16, no. 8, 2000, pp437-452

[6] C. Basdogan, S. De and J. Kim (etc.), "Haptics in minimally invasive surgical simulation and training", IEEE Computer Graphics and Applications, vol. 24, no. 2, 2004, pp. 56-64

[7] D. James and D. Pai, "Artdefo accurate real time deformable objects", Proceedings of the 26th annual conference on Computer graphics and interactive techniques, Los Angeles, USA, 1999, pp. 65-72

[8] C. Monserrat, U. Meier and M. Alcaniz (etc.), "A new approach for the real-time simulation of tissue deformations in surgery simulation", Computer Methods and Programs in Biomedicine, vol. 64, 2001, pp. 77-85

[9] M. Bro-Nielsen, "Finite element modeling in surgery simulation", Proceedings of The IEEE, vol. 86, no. 3, 1998, pp. 490-503

[10] G. Debunne, M. Desbrun, M. P. Cani and A. H. Barr, "Dynamic real-time deformations using space & time adaptive sampling", ACM SIGGRAPH 2001, Los Angeles, USA, pp. 31-36

[11] S. Cotin, H. Delingette and N. Ayache, A hybrid elastic model allowing real-time cutting, deformations and force-feedback for surgery training and simulation, The Visual Computer, vol. 16, no. 8, 2000, pp. 437-452

[12] Y. C. Fung, "Biomechanics: Mechanical properties of living tissues", Second Edition, New York: Springer-Verlag, 1993

[13] R. M. Kenedi, T. Gibson, J. H. Evans and J. C. Barbenel, "Tissues mechanics", Physics in Medicine & Biology, vol. 20, no. 5, 1975, pp. 699-717

[14] W. Maurel, Y. Wu and N. M. T. D. Thalmann, Biochemical models for soft tissue simulation, ESPRIT Basic Research Series, Springer-Verlag, 1998

[15] G. Picinbono, H. Delingette and N. Ayache, "Non-linear anisotropic elasticity for real-time surgery simulation", Graphical Models, vol. 65, no. 5, 2003, pp. 305-321

[16] A. Nurnberger, A. Radetzky and R. Kruse, "Using recurrent neuro-fuzzy techniques for the identification and simulation of dynamic systems, Neurocomputing, vol. 36, 2001, pp. 123-147

[17] A. Duysak, J. J. Zhang and V. Ilankovan, "Efficient modelling and simulation of soft tissue deformation using mass-spring systems", International Congress Series, vol. 1256, 2003, pp. 337-342

[18] L. O. Chua and L. Yang, "Cellular neural network: Theory", IEEE Transactions on Circuits and Systems, vol. 35, no. 10, 1988, pp. 1257-1272

[19] A. Slavova, Cellular Neural Networks: Dynamics and Modelling, Dordrecht, London: Kluwer Academic Publishers, 2003

[20] L. O. Chua and T. Roska, "The CNN Paradigm", IEEE Transactions on Circuits and Systems, vol. 40, No. 3, 1993, pp. 147-156

[21] T. J. Barth, "Aspects of unstructured grids and finite-volume solvers for the Euler and Navier-Stokes equations", AGARD Report 787, pp.6.1-6.61, 1992

[22] D. R. Croft and D. G. Lilley, "Heat transfer calculations using finite difference equations", Applied Science Publishers Ltd, London, 1977

[23] D. Baraff and A. Witkin, "Large steps in cloth simulation", Proceedings of SIGGRAPH'98, pp. 43-54